

R.E. Stoner and R.L. Walsworth  
*Harvard-Smithsonian Center for Astrophysics, Cambridge, MA 02138*  
 (July 29, 2000)

We compared the frequency shift of the  $^{21}\text{Ne}$  Zeeman resonance induced by polarized Rb vapor to the shift induced in the  $^3\text{He}$  Zeeman resonance. The  $^3\text{He}/\text{Rb}$  shift has recently been measured with high precision [18], permitting the conversion of our differential measurement to an absolute value for the  $^{21}\text{Ne}/\text{Rb}$  shift. We report a value of  $\kappa_{21} = 31.8 \pm 2.8$  for the Rb- $^{21}\text{Ne}$  enhancement factor at a temperature of  $124.8^\circ \pm 1.9^\circ\text{C}$ . We propose high-precision differential contact shift measurements, the absolute accuracy of which would be limited by the error in the  $^3\text{He}$  contact shift.

32.80.Bx, 32.60.+i, 84.40.Ik, 34.20.-b, 67.65.+z

## I. INTRODUCTION

Polarization of noble gases by spin exchange with optically pumped alkali metal vapors [1,2] is an important technique for a variety of scientific and technological applications. Polarized noble gases been used for: precise measurements of the neutron spin structure function [3]; neutron polarizers and analyzers [4]; magnetic resonance imaging [5–7]; studies of gas diffusion in porous media [8]; gain media for Zeeman masers [9–11]; and tests of fundamental symmetries [12–15].

New tests of fundamental symmetries using polarized noble gases have recently been proposed. Kosteletzky and Lane recently reported that a  $^{21}\text{Ne}/^3\text{He}$  differential magnetometer could be used to test local Lorentz invariance (LLI) [16]. We have proposed to develop a  $^{21}\text{Ne}/^3\text{He}$  dual noble gas maser to carry out such an LLI test [17].

The spin exchange interaction between alkali and noble gas atoms has been extensively described in the literature [2,18,20–22]. During spin exchange collisions, there is significant overlap of the alkali atom’s valence electron wavefunction with the noble gas nucleus which comprises a Fermi contact interaction of the form

$$H_{int} = \alpha \vec{K} \cdot \vec{S} \quad (1)$$

where  $\vec{S}$  and  $\vec{K}$  are the electron and nuclear spin angular momentum operators, respectively. This interaction leads to exchange of angular momentum between the alkali valence electron and the noble gas nucleus. The valence electron and nucleus experience during the collision a strong magnetic field from the close proximity of their spin magnetic moments. In spite of the small fraction of the time spent in collision, the average magnetic fields experienced by both the alkali valence electron and the noble gas nucleus can be affected if either the alkali or noble gas species is polarized. The resultant change in the Larmor precession frequency for either species, referred to as the contact shift, is expressed in terms of an enhancement factor  $\kappa$ .  $\kappa$  is defined in terms of the *total* shift in the Larmor precession frequencies in co-located spherical distributions of magnetizations, induced both by the contact interaction and by the classical magnetic fields generated by the magnetizations.  $\kappa$  is the ratio of that total frequency shift (contact plus classical magnetization) to the shift that would be induced by the classical magnetization alone.  $\kappa$  can be much greater than unity, increasing with increasing  $Z$  of the noble gas nucleus [20]. In the limit where the formation of alkali-noble gas van der Waals molecules is a negligible part of the spin exchange interaction (true for the experiment reported in this paper), a single enhancement factor describes both the contact shift of the noble gas Zeeman splitting by the alkali atoms, and vice versa. [23]. The frequency shift experienced by noble gas atoms in the presence of polarized alkali atoms, including both the contact shift and the shift due to classical magnetization fields, is

$$\delta\omega_{ng} = (\kappa - 1 + f_{DDF}) \gamma_{ng} \cdot \frac{8\pi}{3} g_S \mu_B [a] \langle S_z \rangle \quad (2)$$

Recall the elementary result that  $\frac{8\pi}{3}M$  is the magnetic field strength inside a magnetized sphere with magnetic dipole moment density  $M$ ; the field is uniform and parallel to the magnetization.  $f_{DDF}$  is a dimensionless factor that accounts for the effect of classical magnetization fields (“distant dipole fields” [18]), and is unity for a spherical distribution of magnetization.  $[a]$  is the number per unit volume of alkali atoms, and  $\gamma_{ng}$  is the gyromagnetic ratio of the noble gas species. For convenience, we define the component of alkali atom magnetization along the magnetic field ( $z$ ) axis,  $M_a$ , as

$$M_a = \hbar \gamma_a [a] \langle S_z \rangle \quad (3)$$

where  $\gamma_a = g_S \mu_B / \hbar = 2\pi \cdot 1.40$  MHz/gauss is the electron gyromagnetic ratio. The alkali nuclear magnetic moments do not contribute to the contact shift, but do affect the distant dipole fields produced by the alkali magnetization distribution. We ignored these effects on the distant dipole fields, since they were too small to bear on the results reported in this work.

In precision measurements, it is important to be able to monitor the absolute polarization of the noble gases. Romalis and Cates [18] demonstrated accurate polarimetry of  $^3\text{He}$  using the Rb Zeeman frequency shift due to Rb- $^3\text{He}$  spin exchange collisions, and made a very precise measurement of the Rb- $^3\text{He}$  enhancement factor. Future use of  $^{21}\text{Ne}$  in precision measurement applications would benefit from the use of contact shift polarimetry, but there is at present no published measurement of the Rb- $^{21}\text{Ne}$  enhancement factor. In this paper we present the first such measurement. We measured the net Larmor frequency shifts, simultaneously impressed by the presence of polarized Rb, on ensembles of polarized  $^3\text{He}$  and  $^{21}\text{Ne}$  precessing in the same [nearly] spherical glass cell. The measurement presented in this paper is not the first in which a ratio of contact shift enhancement factors was determined. Baranga *et. al.* measured the shifts of the Larmor precession frequencies of Rb and K vapors residing in the same cell, induced simultaneously by the presence of polarized  $^3\text{He}$  [19].

The experiment is described in Section II. Determining the ratio of the Rb-induced shifts permitted us to divide out the dependence on Rb magnetization, and express the  $^{21}\text{Ne}$  enhancement factor  $\kappa_{21}$  in terms of the  $^3\text{He}$  enhancement factor  $\kappa_3$ . The very accurate measurement of  $\kappa_3$  by Romalis and Cates determined the absolute contact shift enhancement factor  $\kappa_{21}$ . Analysis of the data is presented in Section III. Suggestions for improved measurements are given in Section IV.

## II. APPARATUS, PROCEDURE, SYSTEM PARAMETERS

We employed a  $^{21}\text{Ne}/^3\text{He}$  dual noble gas Zeeman maser to establish simultaneous precession of the  $^{21}\text{Ne}$  and the  $^3\text{He}$  in the same sealed glass cell. The  $^{21}\text{Ne}/^3\text{He}$  maser is a new device that will be described elsewhere; that description is summarized here. Figure 1 is a schematic representation of the maser. Circularly polarized light resonant with the Rb D1 transition (795 nm) is generated by a 30 W laser diode array (LDA); the light is directed onto a 1.4 cm dia [near-] spherical sealed glass cell containing 228 torr of  $^{21}\text{Ne}$ , 266 torr of  $^3\text{He}$ , 31 torr of  $\text{N}_2$ , and Rb metal of natural isotopic composition [24]. The LDA light propagates along the axis of a uniform magnetic field of strength 3 Gauss. The field is generated by a precision solenoid/ $\mu$ -metal-shield system capable of producing a 3 G magnetic field with  $\leq 35$   $\mu\text{G}/\text{cm}$  magnetic field gradients, with no gradient shimming. The main solenoid was driven using a current source capable of  $\sim 3$  ppm stability over timescales of order 1000 sec. The glass cell was heated both by the LDA light and blown hot air to a temperature of  $(124.8 \pm 1.9)^\circ\text{C}$  (see Sec. III). The temperature of the air surrounding the cell was controlled to about 43 mK RMS. The total output power of the LDA was actively controlled to about a part in  $10^4$ .

The Rb was polarized by optical pumping; the resulting Rb electron polarization was very close to unity. The output power of the LDA was about 30W, so that even though it had a very broad ( $\sim 1.5$  nm) linewidth, the on-resonant optical power was roughly 0.5 W. Thus, the optical pumping rate was  $> 10^5$  photon absorptions per sec per Rb atom. The rate of Rb polarization destruction events per Rb atom in the cell was  $< 10^3$   $\text{sec}^{-1}$  so that the Rb electron polarization was greater than 0.99. Pickup coils wound in series were placed in close proximity to the cell. The coils were excited by the magnetic flux associated with the precession of the polarized noble gases. The coils were part of a tuned resonant circuit with resonances at both noble gas precession frequencies. The large current flow induced in the pickup coils by resonant excitation resulted in magnetic fields oscillating at the noble gas nuclear Larmor frequencies being impressed back on the precessing atoms. This feedback resulted in steady state maser operation.

$^{21}\text{Ne}$  has nuclear spin  $3/2$ , and thus a quadrupole moment. The quadrupole moments of the  $^{21}\text{Ne}$  ensemble interact coherently with electric field gradients at the glass cell walls, shifting the four Zeeman energy levels so as to split the three [otherwise degenerate] dipole transitions [25]. The splitting is proportional to  $\delta\omega_Q \propto 3\cos^2\theta - 1$ , where  $\theta$  is the angle of the cell's symmetry axis with the magnetic field. We oriented the cell as close as possible to the "magic angle"  $\cos\theta = \sqrt{1/3}$  to minimize the quadrupole splitting. The quadrupole wall shifts in the cell were not measured; however, computer simulations indicate that without proper cell orientation, realistic-sized splittings could disrupt  $^{21}\text{Ne}$  maser oscillation. In any case,  $^{21}\text{Ne}$  maser oscillation with steady-state amplitude was attained. We observed a small ( $\sim 10$   $\mu\text{Hz}$ ) sinusoidal modulation of the  $^{21}\text{Ne}$  maser frequency. The period of the modulation was about 16 hr. We speculate that the modulation was a consequence of remnant quadrupole splitting resulting from cell orientation error. In any case, the effect was small, with a period much longer than the duration of our contact shift measurements, and thus was not a source of significant systematic error.

The  $^3\text{He}$  and  $^{21}\text{Ne}$  maser signals were presented to a low-noise preamplifier. The preamp output was then analyzed using lockin amplifiers, which were referenced to a set of synchronized signal generators tuned near the noble gas

maser frequencies and locked to an H-maser-derived 5 MHz signal. The phases of both noble gas masers' precession were recorded digitally at a sample rate of 1 Hz. The A/D sampling trigger was also derived from the master 5 MHz reference.

The measurements consisted of observing the maser phases during a series of reversals of the direction of the Rb polarization. The Rb polarization was reversed by rotation of the quarter-wave plates (Fig. 1) and was typically achieved in  $\leq 20$  sec. The total duration of a set of reversals was about 1000 sec., limited by magnetic field stability as well as the extent to which the noble gas masers' steady states were disrupted by the alternating Rb polarization. Two sets of reversal data were acquired. Clear changes in the slopes of the phase curves were precisely correlated with reversal of the Rb polarization direction; these frequency changes were the result of the contact shift combined with the [classical] shift due to the Rb magnetization distribution. The change of noble gas maser oscillation frequency induced by Rb polarization reversal was about 44 mHz for  $^{21}\text{Ne}$  maser and 71 mHz for the  $^3\text{He}$  maser.

### III. DATA AND ANALYSIS

Phase data for the second of the two measurement scans are shown in Figs. 2 and 3. We model the  $^{21}\text{Ne}$  phase  $\varphi_{21}$  (see Fig. 2) and the  $^3\text{He}$  phase  $\varphi_3$  (see Fig. 3) acquired by the lockin amplifiers as evolving according to the following equations:

$$\begin{aligned}\varphi_{21} &= \varphi_{21,o} + \gamma_{21} B_o t - 2\pi \nu_{ref,21} + \gamma_{21} \int_0^t dt' \delta B(t') + (\kappa_{21} - 1 + f_{DDF}) \gamma_{21} \frac{8\pi}{3} \int_0^t dt' M_{Rb}(t') \\ \varphi_3 &= \varphi_{3,o} + \gamma_3 B_o t - 2\pi \nu_{ref,3} + \gamma_3 \int_0^t dt' \delta B(t') + (\kappa_3 - 1 + f_{DDF}) \gamma_3 \frac{8\pi}{3} \int_0^t dt' M_{Rb}(t')\end{aligned}\quad (4)$$

where:  $\gamma_{21}$  ( $\gamma_3$ ) is the gyromagnetic ratio of Ne (He);  $\kappa_{21}$  ( $\kappa_3$ ) is the enhancement factor for Ne (He);  $f_{DDF}$  is the dimensionless factor to account for the classical magnetic field due to the Rb magnetization;  $\nu_{ref,21}$  and  $\nu_{ref,3}$  are the reference frequencies presented to the lockin amplifiers;  $B_o$  is the time-average magnetic field strength over the time interval;  $\delta B$  is the time-dependent deviation of the magnetic field from its mean value; and  $M_{Rb}$  is the Rb magnetization. Note that independent maser frequency measurements determined the ratio of the two gyromagnetic ratios,  $\gamma_3/\gamma_{21}$ , to an accuracy much better than 1 ppm. Also, the effects of magnetic fields due to noble gas magnetization fields on the phases have been neglected in comparison to the contact shift effects; this is reasonable for the noble gas magnetizations of this experiment (see below).

Magnetic field drift occurred over the course of the measurement scan. However, the  $^{21}\text{Ne}$  and  $^3\text{He}$  masers are co-located magnetometers, so that we can construct a data set from which the effects of magnetic field drift and Rb distant dipole fields have been removed. We define

$$\Delta\varphi \equiv \varphi_3 - \frac{\gamma_3}{\gamma_{21}} \varphi_{21} \quad (5)$$

It is easily shown that

$$\Delta\varphi = \varphi_{3,o} - \varphi_{21,o} + 2\pi \left( \frac{\gamma_3}{\gamma_{21}} \nu_{ref,21} - \nu_{ref,3} \right) t + (\kappa_3 - \kappa_{21}) \gamma_3 \frac{8\pi}{3} \int_0^t dt' M_{Rb}(t') \quad (6)$$

Aside from a trivial phase offset and known linear phase evolution,  $\Delta\varphi$  reflects the action of the Rb contact shifts only: phase evolution due to magnetic fields is subtracted off. This combined phase profile is plotted in Fig. 4. As seen in Fig. 4, the phase evolution due to the contact shift was a piecewise-linear "sawtooth" profile. Since our measurement is derived from computing the differences in slopes between adjacent linear regions of the curve, removal of constant and linear dependence from the phase data had no effect on the measurement. Thus, our plots of the phase data shown in Figs. 2, 3, and 4 are displayed with mean value and mean slope of zero.

If the Rb magnetization were known, one could immediately deduce  $\kappa_{21}$  using eqn (6). Even though the Rb electron spin polarization was very close to unity, the density was not known *a priori*. It was therefore necessary to consider the ratio of contact shifts impressed on the  $\varphi_{21}$  and the  $\Delta\varphi$  phase curves, and then determine the temperature self-consistently.

The data were analyzed in two ways which yielded essentially identical results. First, we computed the average changes in slope of the phase curves  $\varphi_{21}$  and  $\Delta\varphi$ , caused by the reversals of the Rb magnetization. That is, a least-squares linear fitting routine was used to extract the slope of each piecewise linear region of the phase curves. The differences in slope of adjacent regions was then recorded for each of the phase curves. The mean absolute values

of the slope differences were then computed for each data set. We define  $M_{21}$  as the mean of the absolute value of the slope differences for  $\varphi_{21}$ , and  $\Delta M$  as that for the  $\Delta\varphi$  profile. The uncertainties were estimated as the standard deviation of the mean in the slope differences' absolute values.

We define the ratio of mean slope changes as  $\mathcal{R} \equiv M_{21}/\Delta M$ . The weighted average value for  $\mathcal{R}$  from the two data sets was  $\mathcal{R} = 0.1262 \pm 0.0025$  where a one-sigma uncertainty is reported. The uncertainty was almost entirely due to that in  $M_{21}$ . The fractional uncertainty in  $\Delta M$  for both of the data sets was  $< 0.1\%$ . This indicates that Rb polarization reversal was achieved to high precision and that the Rb magnetization was stable to better than 0.1% over the course of the measurements. The fractional uncertainty in  $M_{21}$  was much larger,  $\sim 2\%$ , caused by the effects of magnetic field drift. In principle, we could have analyzed the  $\varphi_3$  profile rather than  $\varphi_{21}$ , but magnetic field drift effects were  $\gamma_3/\gamma_{21} = 9.65$  times larger on  $\varphi_3$  than  $\varphi_{21}$ , making it impractical to extract slope data from  $\varphi_3$  directly (see Fig. 3).

In our analysis we did not account for possible variations in frequency due to changes in the noble gas longitudinal polarization that occurred in the course of a measurement. The magnetization of the noble gases created magnetic fields which varied in time during the course of the each of the two measurement scans, as evidenced by [small] maser amplitude changes observed during the scans. A given maser's magnetization field could not affect its own frequency, since magnetization fields were parallel to the magnetization in the near-spherical cell. However, each maser's frequency was shifted by the other's magnetization, and such shifts did not subtract out of  $\Delta\varphi$  as did magnetic field drift. The noble gas polarizations underwent both slow drift as well as variations correlated with the Rb polarization reversals. The small uncertainty in the  $\Delta\varphi$  slope differences proves that frequency variations due to slow drift in the noble gas magnetizations had negligible effect. We also determined that the variations of the noble gas polarization caused by the periodic Rb polarization reversal had negligible effect on the contact shift measurement. Periodic reversal of the Rb polarization (i.e., "square wave" modulation of the Rb polarization) induced a "sawtooth wave" modulation (i.e., integrated square wave) on the noble gas polarizations of peak-to-peak amplitude approximately  $\gamma_{SE}\tau$ , where  $\gamma_{SE}$  is the Rb-noble gas spin exchange rate per noble gas atom, and  $\tau$  = time between Rb polarization reversals. Thus, the varying noble gas polarizations induced large changes in the maser frequencies over a measurement period: we estimate that a 2.8 mHz shift was induced on the  $^3\text{He}$  maser by the  $^{21}\text{Ne}$  polarization variation and a 0.7 mHz shift was induced on the  $^{21}\text{Ne}$  maser by the  $^3\text{He}$  polarization variation. However, given a constant time interval  $\tau$  between Rb polarization reversals, the *average* frequency shifts due to the Rb-driven noble gas polarization variations did not change from one period to the next, thus they subtracted out in the calculation of the period-to-period frequency changes  $M_{21}$  and  $\Delta M$ . We conclude that noble gas polarization-induced magnetic fields had no systematic effect on the measurement of  $\mathcal{R}$ .

It is easy to show from eqns (4) and (6) that the ratio  $\mathcal{R}$  can be interpreted as

$$\mathcal{R} = \left| \frac{\gamma_{21}}{\gamma_3} \cdot \frac{\kappa_{21} + (f_{DDF} - 1)}{\kappa_3 - \kappa_{21}} \right| \quad (7)$$

where it is seen that dependence on the Rb magnetization divided out. The value and estimated uncertainty for  $\mathcal{R}$  can then be used to compute the value and uncertainty of the desired contact shift enhancement factor for  $^{21}\text{Ne}$ ,  $\kappa_{21}$ , though the system temperature must be known because  $^3\text{He}$  contact shift  $\kappa_3$  is temperature-dependent.  $\kappa_{21}$  and the system temperature must be determined self-consistently, and the effect of classical magnetization fields must be accounted for: these questions are addressed below.

We now consider the second method of analyzing the data to obtain a value for  $\mathcal{R}$ , which yielded essentially the same results as the above approach. While this second method is slightly more complex, it is useful because it provides a framework for estimating the size of magnetic field drift in the present measurement. This second method of extracting a value of  $\mathcal{R}$  from the data considers the phase data sets to be  $N$ -component vectors (denoted by a tilde), where  $N \equiv$  number of data in the set ( $\sim 10^3$  for each of the two scans). We use the  $\Delta\varphi$  profile as a model of the shape of the Rb magnetization-induced phase (see eqn 6). We then seek to describe the  $\tilde{\varphi}_{21}$  profile vector as a linear combination of elements of a partial basis of orthonormal vectors. The partial basis included an element corresponding to the [normalized]  $\Delta\varphi$  profile ( $\equiv \tilde{V}_0$ ). Additional basis vectors orthogonal to it,  $\{\tilde{V}_i\}_{i=1, N_b-1}$  were derived from  $\Delta\varphi$  and Legendre polynomials  $\{P_i\}_{i=0, N_b-1}$  using Gram-Schmidt orthogonalization [27]. The number of basis vectors  $N_b$  was of order  $10^1$ , whereas the dimension of the vector space  $N$  was of order  $10^3$ , so  $N_b \ll N$ , and we find:

$$\tilde{\varphi}_{21} = \sum_{i=0}^{N_b-1} a_i \tilde{V}_i \quad (8)$$

The coefficient of  $\tilde{V}_0$  in this linear combination,  $a_0$ , was proportional to the value for  $\mathcal{R}$  obtained from that data set. The coefficients of the linear combination were determined using linear least squares fitting and by simple projection

of  $\tilde{\varphi}_{21}$  onto the vectors of the partial basis, with identical results. The number of elements in the basis set was varied, but the coefficients obtained from the least squares fit remained the same regardless of the size of the basis set.

Using this second data analysis method, we thus determined two values of  $\mathcal{R}$ , one from each data set. It was not possible to estimate uncertainties for the individual values of  $\mathcal{R}$  from the vector analysis method. Uncertainty estimates from the least squares analyses were unrealistically small because the vector analysis could not account for the effect of a non-zero projection of the magnetic field drifts along the Rb magnetization-induced phase profile vectors. We take the value of  $\mathcal{R}$  to be the mean of the results for the two data sets, and we coarsely estimate the uncertainty of  $\mathcal{R}$  as the deviation of the two values, to obtain  $\mathcal{R} = 0.1287 \pm 0.0036$ . This result agrees well with that of the first method of data analysis. For computing  $\kappa_{21}$  we will use the result from the first method of analysis since the error estimate is probably more reliable.

We can compute the magnetic field drift profile by subtracting from  $\tilde{\varphi}_{21}$  its projection on the Rb magnetization basis profile  $\tilde{V}_0$ :

$$\delta\tilde{B} = \frac{1}{\gamma_{21}} \frac{d}{dt} \left( \tilde{\varphi}_{21} - \left( \tilde{\varphi}_{21} \cdot \tilde{V}_0 \right) \tilde{V}_0 \right) \quad (9)$$

Note that the profile  $\delta\tilde{B}$  is the magnetic field drift *orthogonal* to  $\tilde{V}_0$ . The drift profile from the second data set is plotted in Fig. 5; the time derivative of the [discretely sampled] profile was estimated by finite difference. Note that the field was stable to about  $\pm 3$  ppm RMS.

Having obtained a value for  $\mathcal{R}$ , we can then solve eqn (7) for  $\kappa_{21}$  in terms of measured parameters, since  $\kappa_3$  is known [18]. However,  $\kappa_{21}$  is expected to be temperature-dependent [18,20] and so the temperature at which the experiment was carried out must be reported along with the value of  $\kappa_{21}$ . The Rb and noble gas temperature indicated by the hot air temperature control system was in error, because: the absolute calibration was poorly known; and the cell was heated by the LDA to a temperature higher than that indicated by the control system. Thus, it was necessary to deduce the noble gas/Rb vapor temperature from the contact shift data, and the known  $^3\text{He}$  enhancement factor (with its known temperature dependence), in a self-consistent way. This was achieved by first noting that the mean slope change  $\Delta M$  is related to the enhancement factors and the Rb magnetization via

$$\Delta M = 2\gamma_3 \frac{8\pi}{3} |(\kappa_3 - \kappa_{21}) M_{Rb}(T)| \quad (10)$$

where  $|M_{Rb}(T)|$  (see eqn (3) above) is a known function of temperature. The Rb number density  $[Rb]$  is related to temperature by [26]

$$[Rb] = \frac{10^{9.318 - \frac{4040}{T}}}{(1.38 \cdot 10^{-17}) \cdot T} \text{cm}^{-3} \quad (T \text{ in } ^\circ\text{K}) \quad (11)$$

The measured temperature dependence of the  $^3\text{He}$  enhancement factor is [18]

$$\kappa_3 = 4.52 + 0.00934 [T (^\circ\text{C})] \quad (12)$$

Substituting (11) and (3) into (10) yields an equation relating  $\kappa_{21}$  and temperature (and known/measured parameters). Substituting (12) into (7) yields another equation relating  $\kappa_{21}$  and temperature. This system of two [nonlinear] equations and two unknowns can be solved to yield the temperature and  $\kappa_{21}$ . The temperature determination depends strongly on the enhancement factor, while the enhancement factor determination depends only weakly on the temperature (via the known temperature dependence of  $\kappa_3$ ). Thus, an iterative method to compute the temperature rapidly converges: an initial guess for the temperature enables calculation of  $\kappa_{21}$ , which in turn permits calculation of the Rb magnetization and thus the system temperature. This corrected temperature is used to re-compute a better estimate for  $\kappa_{21}$ , which is used to re-compute a better estimate of the Rb magnetization, etc.

Using the result  $\mathcal{R} = 0.1262 \pm 0.0025$  from the slope difference analysis, we determine the contact shift enhancement factor for Rb and  $^{21}\text{Ne}$  to be  $\kappa_{21} = 31.8 \pm 2.8$  at a temperature of  $(124.8 \pm 1.9)^\circ\text{C}$ . Note that the noble gas/Rb vapor temperature is much higher than the value of  $112^\circ\text{C}$  indicated by the hot air temperature control system, presumably the result of heating by the laser diode array. We are not aware of a previous measurement of the Rb- $^{21}\text{Ne}$  contact shift. Walker estimated the Rb- $^{21}\text{Ne}$  enhancement factor to be 38, and the ratio of the Rb- $^{21}\text{Ne}$  and Rb- $^3\text{He}$  enhancement factors to be 4.3 [20]. We report this ratio to be  $5.6 \pm 0.5$ .

The 3% uncertainty in  $\mathcal{R}$  dominates other sources of error, inducing a 9% uncertainty in  $\kappa_{21}$ . The contribution to the uncertainty in  $\kappa_{21}$  resulting from the 1.5% uncertainty in the He enhancement factor  $\kappa_3$  is only 1.5%, which is negligible. The uncertainty in temperature induced a 0.3% uncertainty in  $\kappa_{21}$ . To the extent that the cell could be described as an ellipsoid of revolution, its deviation from sphericity induced an uncertainty of 0.15% in  $\kappa_{21}$  with zero systematic correction.

The claim of zero systematic correction of the classical magnetization field shift for a ellipsoidal cell is justified by noting that: i) the classical magnetization field inside an ellipsoid of uniform magnetization is uniform, with its magnitude depending on the ellipsoid's shape and the relative orientation of the ellipsoid major axis and the magnetization vector; and ii) when the ellipsoid major axis is oriented at the magic angle  $\theta_m = \cos^{-1}(1/\sqrt{3})$  with respect to the magnetization direction, the component of the classical magnetization field parallel to the magnetization is exactly that of a spherical distribution with the same magnetization, regardless of the ellipsoid's shape. We oriented the cell at  $\theta_m$  in order to suppress quadrupole wall shifts, with an uncertainty of about  $10^\circ$ . The  $10^\circ$  uncertainty in orientation leads to the estimated uncertainty of 0.15% in  $\kappa_{21}$  due to measured asphericity of the cell.

#### IV. SUGGESTIONS FOR IMPROVED MEASUREMENTS; CONCLUSIONS

There are straightforward improvements that could be implemented to reduce the uncertainty in the present measurement. The experiment was conducted in the course of developing a  $^{21}\text{Ne}/^3\text{He}$  dual Zeeman maser, so that opportunity for taking contact shift data was very limited. A factor of three improvement in the result could easily be achieved just by taking ten times more data. Active field stabilization using an independent magnetometer [18] would essentially eliminate field drift, reducing statistical uncertainty in the measurement to that due to phase noise, a factor of  $> 0.03/0.001 = 30$  reduction. Active field stabilization would also permit a reduction in the phase noise since the signal acquisition bandwidth could be reduced by at least a factor of 3, so that the statistical uncertainty could be reduced by about a factor of 300 compared to the present experiment. This uncertainty would already be less than the uncertainty contributed by cell asphericity (0.15%). However, the absolute uncertainty in the Rb- $^{21}\text{Ne}$  contact shift enhancement factor  $\kappa_{21}$  would then be limited by the uncertainty in that for He,  $\kappa_3$ , 1.5%, whereas the ratio  $\kappa_{21}/\kappa_3$  would be known to an uncertainty of only a few tenths of one percent.

It should be possible to measure ratios of alkali-noble gas enhancement factors to a level well below a part in  $10^3$  if one could completely eliminate effects of the classical magnetization field shift. We have already shown that one can use differential magnetometry to obtain data from which classical magnetization field shifts are eliminated to high precision. It can be shown that using a three-species noble gas maser, one could measure the contact shift enhancement factor of a third species if the other species' enhancement factors are known, *independent of the classical magnetization field shift*. Even though it has not yet been done, we believe it is a straightforward matter to implement a three-species maser in a single-bulb glass cell.

A comprehensive set of contact shift data would serve as a probe of noble gas-alkali interaction potentials [20]. A program using multi-species noble gas masers to measure contact shift ratios could be implemented using  $^{129}\text{Xe}$ ,  $^{83}\text{Kr}$ ,  $^{21}\text{Ne}$ , and  $^3\text{He}$  along with K, Cs, and Rb in turn. Na would be a poor candidate for use in a noble gas maser because of its relatively low vapor pressure. The remaining stable noble gas isotope,  $^{131}\text{Xe}$ , cannot be used with the other noble gases in a multi-species maser because its nuclear dipole moment has a sign opposite to that of the others (making it impossible to achieve a population inversion simultaneously with the other species). However, it may be possible to measure the  $^{131}\text{Xe}$  precession frequency in free induction decay in the presence of two other noble gas masers. There are no other stable noble gas isotopes having non-zero nuclear spin.

Contact shift ratios would be converted to absolute values for enhancement factors by using the measured values for  $^3\text{He}/\text{Rb}$  [18] and  $^3\text{He}/\text{K}$  [19]. The enhancement factor for  $^3\text{He}/\text{Cs}$  has not yet been measured.

Measuring contact shift ratios to a few parts in  $10^4$  could proceed as follows: one would first measure the ratio of the enhancement factors of  $^{83}\text{Kr}$  and  $^{129}\text{Xe}$  to each other. The contact shift enhancement factors for  $^{83}\text{Kr}$  and  $^{129}\text{Xe}$  are estimated by Walker to be about 230 and 730, respectively [20]. Using an independent magnetometer with the colocated Xe-Kr masers, the ratio of the [large] enhancement factors of Xe and Kr could be measured to a few parts in  $10^4$  even if the classical magnetization field were accounted for only to the 10% level (which can be done trivially- a  $\sim 1\%$  accounting is claimed in this work). Triple masers using Kr and Xe, along with  $^{21}\text{Ne}$  and  $^3\text{He}$  in turn would yield high-precision measurements of the ratios of all the enhancement factors; the known enhancement factor for He would then determine the absolute values of the other enhancement factors. Temperature dependences could of course also be measured. In particular, enhancement factor ratios as a function of density (normalized to some experimental reference density) could be determined to very high precision. Improved cell thermometry would eliminate the need to depend on a temperature-density calibration [26] to determine the cell temperature. Also, for very high precision measurements, control of the noble gas magnetization fields would have to be maintained more carefully than in the present work; in particular, the time between polarization reversals could be decreased in order to increase the relative size of the contact shifts in comparison to noble gas polarization induced frequency shifts. It might also be important to account carefully for the contribution of van der Waals molecule formation to the contact frequency shifts.

Finally, we remark that a two species maser using  $^3\text{He}$  and  $^{21}\text{Ne}$  has been proposed for a high precision test of

local Lorentz invariance (LLI) [17], in which Rb-noble gas contact shifts would be an important systematic effect. Adding a co-located  $^{129}\text{Xe}$  maser would provide a high precision *in situ* measurement of the Rb magnetization. With part-in- $10^4$  knowledge of the enhancement factors, the systematic effects of contact shifts on a search for LLI violation could be rendered negligible with the use of the  $^{129}\text{Xe}$  maser "co-polarimeter".

We thank T. Chupp for the use of the  $^{21}\text{Ne}/^3\text{He}$  cell, and gratefully acknowledge D. Phillips and D. Bear for useful conversations.

- 
- [1] M.A. Bouchiat, T.R. Carver, and C.M. Varnum, Phys. Rev. Lett. **5**, 373 (1960)
  - [2] T. Walker and W. Happer, Rev. Mod. Phys. **69**, 629 (1997)
  - [3] K. Abe *et al.*, Phys. Rev. Lett. **79**, 26 (1997); Phys. Lett. B **404**, 377 (1997)
  - [4] G.L. Greene, A.K. Thompson, and M.S. Dewey, Nucl. Inst. Meth. A **356**, 177 (1995)
  - [5] M.S. Albert, G.D. Cates, B. Driehuys, W. Happer, B. Saam, C.S. Springer Jr., and A. Wishnia, Nature **370**, 199 (1994); H. Middleton, L.W. Hedlund, G.A. Johnson, K. Juwan, J. Schwartz, Magn. Reson. Med. **33**, 271 (1995)
  - [6] G. R. Davies, T. K. Halstead, R. C. Greenhow, and K. J. Packer, Chem. Phys. Lett. **230**, 239 (1994); B. R. Patyal et al., J. Magn. Reson. **126**, 58 (1997); M. Bock, Magn. Reson. Med. **38**, 890 (1997); D. M. Schmidt et al., J. Magn. Reson. **129**, 184 (1997); H.U. Kauczor, R. Surkau, T. Roberts, Euro. Radiol. **8**, 820 (1998), and references therein.
  - [7] C.H. Tseng, G.P. Wong, V.R. Pomeroy, R.W. Mair, D.P. Hinton, D. Hoffmann, R.E. Stoner, F.W. Hersman, D.G. Cory, and R.L. Walsworth, Phys. Rev. Lett. **81**, 3785 (1998)
  - [8] R.W. Mair, D.G. Cory, S. Peled, C.H. Tseng, S. Patz, R.L. Walsworth, J. Magn. Reson. **35**, 478 (1998); R.W. Mair, G.P. Wong, D. Hoffmann, M.D. Hurlimann, S. Patz, L.M. Schwartz, R.L. Walsworth, Phys. Rev. Lett. **83**, 3324 (1999).
  - [9] T.E. Chupp, R.J. Hoare, R.L. Walsworth, and Bo Wu, Phys. Rev. Lett. **72**, 2363 (1994)
  - [10] R.E. Stoner, M.A. Rosenberry, J.T. Wright, T.E. Chupp, E.R. Oteiza, and R.L. Walsworth, Phys. Rev. Lett. **77**, 3971 (1996)
  - [11] M.V. Romalis and W. Happer, Phys. Rev. A **60**, 1385 (1999)
  - [12] D. Bear, T.E. Chupp, K. Cooper, S. DeDeo, M. Rosenberry, R.E. Stoner, and R.L. Walsworth, Phys. Rev. A **57**, 5006 (1998)
  - [13] T.E. Chupp and R.J. Hoare, Phys. Rev. Lett. **64**, 2261 (1990)
  - [14] T.E. Chupp, R.J. Hoare, R.A. Loveman, E.R. Oteiza, J.M. Richardson, M.E. Wagshul, A.K. Thompson, Phys. Rev. Lett. **63**, 1541 (1989)
  - [15] T.G. Vold, F. Raab, B. Heckel, and E.N. Fortson, Phys. Rev. Lett. **52**, 2229 (1984)
  - [16] V.A. Kostelecky and C.D. Lane, Phys. Rev. D **60**, 116010 (1999)
  - [17] R.E. Stoner, in *CPT and Lorentz Symmetry*, V.A. Kostelecky, ed., World Scientific, Singapore (1999), p. 201
  - [18] M.V. Romalis and G.D. Cates, Phys. Rev. A **58**, 3004 (1998)
  - [19] A. Ben-Amar Baranga, S. Appelt, M.V. Romalis, C.J. Erickson, A.R. Young, G.D. Cates, and W. Happer, Phys. Rev. Lett. **80**, 2801 (1998)
  - [20] T.G. Walker, Phys. Rev. A **40**, 4959 (1989)
  - [21] W. Happer and W.A. van Wijngaarden, Hyperfine Int. **38**, 435 (1987)
  - [22] W. Happer, Rev. Mod. Phys. **44**, 169 (1972)
  - [23] S.R. Schaefer, G.D. Cates, Ting-ray Chien, D. Gonatas, W. Happer, and T.G. Walker, Phys. Rev. A **39**, 5613 (1989)
  - [24] T.E. Chupp, private communication
  - [25] W. Zu, S.R. Schaefer, G.D. Cates, and W. Happer, Phys. Rev. A **37**, 1161 (1988)
  - [26] C.B. Alcock, V.P. Itkin, and M.K. Horrigan, Canadian Metallurgical Qtrly **23**, 309 (1984)
  - [27] K. Hoffman and R. Kunze, *Linear Algebra*, Prentiss-Hall, Inc. (1971), p. 280

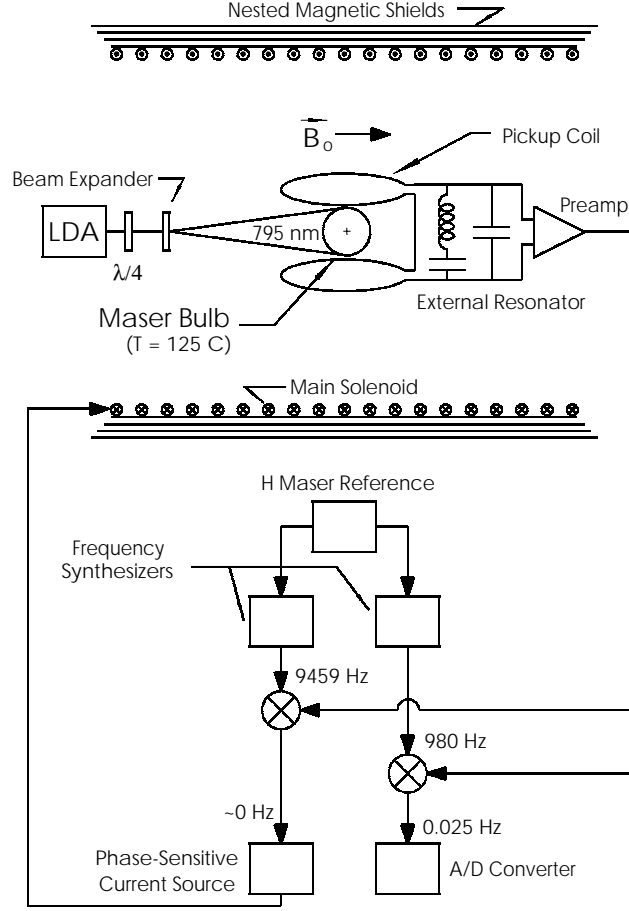


FIG. 1. The  $^{21}\text{Ne}/^3\text{He}$  dual Zeeman maser. The device operates similarly to the  $^{129}\text{Xe}/^3\text{He}$  maser [10], except that the  $^{21}\text{Ne}/^3\text{He}$  maser employs a single- rather than a double-bulb cell. Co-located ensembles of noble gas atoms are polarized by spin exchange collisions with optically pumped Rb atoms. Precession of polarized atoms excites current in nearby inductive pickup coils, which are part of a circuit tuned with resonances near the Larmor precession frequencies of the two noble gas species. The current induces magnetic fields which act back on the precessing atoms, providing feedback for maser oscillation.

fig2.eps

FIG. 2. Example  $^{21}\text{Ne}$  maser phase profile from one (of two) measurement scans. Phase dependence linear in time has been removed.

fig3.eps

FIG. 3. Example  $^3\text{He}$  maser phase profile measured simultaneously with the data of Fig. 2. Phase dependences linear in time have been removed. Note the considerable distortion in this phase curve due to magnetic field drift.

fig4.eps

FIG. 4. The combined phase  $\Delta\varphi$  of the two masers as per eqn (5). This profile is proportional to the phase variation induced by the Rb-noble gas contact shift alone. The sawtooth shape arises from periodic reversal of the Rb polarization, which reverses the Rb-noble gas contact frequency shift. The highly regular shape of the difference curve reflects the fact that magnetic field drift effects are subtracted out.



FIG. 5. Magnetic field drift during the measurements of Figs. 2 and 3, computed from eqn (9). The field strength was 3 G, so that the fractional RMS stability of the magnetic field was about 3 ppm. Field drift was the dominant source of experimental error.